Multibaseline Phase Unwrapping With a Refined Parametric Pure Integer Programming for Noise Suppression

Jiawei Yue [ID], Qihuan Huang [ID], Hui Liu, Ziqi He, and Hanwen Zhang

Abstract—**Multibaseline phase unwrapping (MBPU) is a key procedure of interferometric synthetic aperture radar (InSAR). However, phase noise is a factor still challenging the MBPU accuracy. This article presents a refined pure integer programming (RPIP)-based MBPU method. In this method, a new parameter is introduced through considering the statistical information of the interferometric phase, which is adopted to improve the tolerance of phase noise. We also provide an effective path for searching of the ambiguity set. Theoretical analysis and experimental results show that, compared with the PIP method, unwrapping errors of the RPIP method is reduced by 60%.**

Index Terms—**Interferometric synthetic aperture radar (InSAR), multibaseline (MB), noise robustness, parametric, phase unwrapping (PU).**

I. INTRODUCTION

INTERFEROMETRIC synthetic aperture radar (InSAR) is a key technology to obtain the high-precision digital elevation model (DEM) and surface deformation [1], [2], [3]. However, the interferometric phase obtained by InSAR is in the principal interval $(-\pi, \pi]$, which is called the wrapped phase. Therefore, phase unwrapping (PU), as a key technical procedure, must be applied to recover the absolute phase [4]. The single-baseline PU (SBPU) method [5] is limited by the phase continuity assumption, which makes it not applicable for large phase gradient, especially the phase jumps, or severe displacement phase [6], [7]. The multibaseline PU (MBPU) methods extend the ambiguity interval of SBPU by utilizing MB datasets, which can eliminate the phase continuity assumption [8], [9].

Jiawei Yue, Qihuan Huang, Ziqi He, and Hanwen Zhang are with the School of Earth Sciences and Engineering, Hohai University, Nanjing 211100, China (e-mail: InSAR@hhu.edu.cn).

Hui Liu is with the College of Surveying and Geo-Information, North China University of Water Resources and Electric Power, Zhengzhou 450046, China (e-mail: liuhui_cehui@ncwu.edu.cn).

MBPU methods can be roughly divided into parametric and nonparametric methods [10]. For the former, the terrain height is estimated as a parameter by the probability density function of the InSAR system, and representative parameter estimation criteria include maximum likelihood (ML) [11] and maximum a posteriori (MAP) [12]. However, in order to obtain high-precision DEM estimation, the relevant parameters of the ML method and MAP methods need to be constantly optimized [13], which is an iterative procedure. Therefore, the latter recover the terrain height by solving the ambiguity set of the interferometric phase constraint equation, which avoids iterative calculation of parameters. The classical Chinese remainder theorem (CRT) nonparametric method obtains the ambiguity set by solving the congruence equations [14]. However, the CRT method is too sensitive to noise [15]. In order to improve the robustness of the CRT method, some improved CRT methods were proposed [16], [17], [18]. In addition, another nonparametric MBPU method based on cluster analysis (CA) is proposed, which improves the noise robustness by using the intercept cluster as the reference intercept of the whole region [19]. Some extended CA methods are used to refine the intercept cluster center to improve the PU accuracy [20], [21], [22]. Although CA-related methods adopt the cluster-by-cluster PU approach, the PU efficiency is still time consuming when the number of baselines or the ambiguity number search space is too large [23]. To improve the efficiency of the MBPU method, the mathematical programming that optimizes objective functions or constraints is integrated into nonparametric MBPU. Liu et al. [24] proposed a mixed-norm MBPU based on linear programming (LP), which decreases the dimension of the variable. Yu and Lan proposed a two-stage programming (TSPA) MBPU method [25], and LP algorithms could be used for solving the ambiguity number of SBPU in the second stage [26]. Note that the decision variables of the LP-based MBPU method are associated with the gradient information [27]. The mixed-integer programming (MIP) model is constructed by introducing a local plane, whose maximum deviation from the real terrain determines the decision variables [28]. Considering the relationship between the interferometric phases of the same pixel under different the pure integer programming (PIP) MBPU method is proposed [29]. The decision variables of the

PIP method only contain ambiguity numbers, which are independent and do not need to be combined with the contextual information [30], [31], thus reducing the memory requirement. However, a straight line, which is directly determined by the intercept, is used to constrain and search the ambiguity set. Actually, due to the phase noise, the ambiguity set candidates could be outside of the constraint line, hence, a wrong phase ambiguity set could be achieved and lead to PU failure.

In this article, a refined PIP (RPIP) MBPU method is proposed. In particular, we modify the model by utilizing the intercept information of the interferometric phase. First, we introduce a new parameter in the model to increase the linear constraints and extend the feasible domain of ambiguity set. Then, instead of searching directly on constraint lines, we introduce a threshold criterion to obtain an ambiguity set. The method has a loose feasible region, and the ambiguity set candidates fall within the feasible region, thus reducing the deviation caused by phase noise.

In Section II, the principle of the PIP method is reviewed and analyzed. Section III describes the RPIP method in detail. Section IV verifies the performance of the RPIP method by simulated and real MB InSAR data. Some conclusions are drawn in Section V.

II. REVIEW OF PIP MBPU METHOD

For the MB InSAR system with the normal baseline (or perpendicular baseline) $B_i(i = 1, 2, \ldots, N)$, the relation between the terrain height $h(s)$ of the sth pixel and its wrapped phase $\varphi_i(s)(i = 1, 2, \ldots, N)$ is

$$h(s) = \frac{\lambda \cdot r(s) \cdot \sin\theta}{4\pi \cdot B_i} \cdot [\varphi_i(s) + 2k_i(s)\pi] \quad (1)$$

where λ is the wavelength, $r(s)$ is the slant range of the sth pixel, θ is the incidence angle, and $k_i(s)$ is the unknown integer ambiguity of the sth pixel in the ith interferogram.

Through introducing the ambiguity height [18] $H_i = \lambda \cdot r(s) \cdot \sin\theta/(2B_i)$, (1) can be simplified into

$$h(s) = k_i(s) \cdot H_i + \frac{\varphi_i(s)}{2\pi} \cdot H_i. \quad (2)$$

In order to preserve integer bytes, the relevant parameters (constant M and the module Γ_i) are involved, which are expressed as $M = gcd(H_1 * 10^n, H_2 * 10^n)/10^n$ (gcd is the greatest common divisor) and $\Gamma_i = H_i/M$. Under different baselines, dividing both sides of (2) by M and transforming it into

$$\frac{h(s)}{M} = k_i(s) \cdot \Gamma_i + r_i(s). \quad (3)$$

Let the last $N-1$ equations in (3) subtract the first one and we then have

$$\text{argmin} \left\| \sum_{i=1}^{N} c_i(s) \cdot |k_i(s)| \right\|_1$$
$$\text{s.t. } A_{N-1 \times N} X_{N \times 1} = R_{N-1 \times 1} \quad (4)$$

where $c_i(s)$ is the coherence coefficient of pixel s, $A_{N-1 \times N}$ is an $N-1 \times N$ incidence matrix, where N denotes the number of interferograms, $X_{N \times 1}$ is the ambiguity set vector
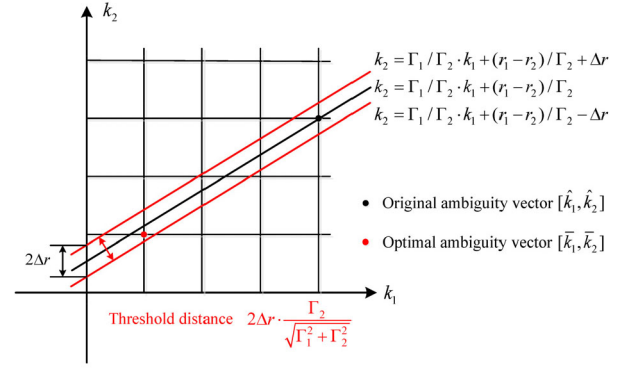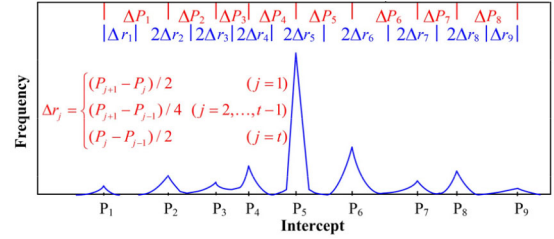

Fig. 1. Schematic of the RPIP model.

Fig. 2. Schematic of determining Δr_j.

$[k_1, k_2, \ldots, k_N]^T$, and $R_{N-1 \times 1}$ is an observation remainder difference vector, which are defined as

$$A_{N-1 \times N} = \begin{bmatrix} \Gamma_1 & -\Gamma_2 & 0 & \cdots & 0 \\ \Gamma_1 & 0 & -\Gamma_3 & \cdots & 0 \\ \vdots & \vdots & \vdots & \vdots & \vdots \\ \Gamma_1 & 0 & 0 & \cdots & -\Gamma_N \end{bmatrix}$$

$$R_{N-1 \times 1} = \begin{bmatrix} r_2(s) - r_1(s) \\ r_3(s) - r_1(s) \\ \vdots \\ r_N(s) - r_1(s) \end{bmatrix}.$$

However, A is a matrix of full-rank rows, (4) can be treated as L^1-norm integer LP (ILP) problem with infinite solutions. Some related search algorithms can obtain the optimal integer solution of (4), such as the well-known branch-and-bound or cutting plane algorithms. Actually, phase noise could destroy $r_i(s)$, which may cause the ambiguity set obtained through search to deviate from the actual value [32], [33].

III. RPIP MBPU METHOD

Considering the phase noise, we need to set an upper limit on the tolerance of PU error, (4) can be reformulated as

$$\text{argmin} \left\| \sum_{i=1}^{N} c_i(s) \cdot |k_i(s)| \right\|_1$$
$$\text{s.t. } | A_{N-1 \times N} X_{N \times 1} - R_{N-1 \times 1} | \leq U_{N-1 \times 1} \quad (5)$$

where $U_{N-1 \times 1}$ is a PU error tolerance vector, which is composed of different parameters Δr, we will provide a detailed description of the determination and allocation of Δr in Section III-A.
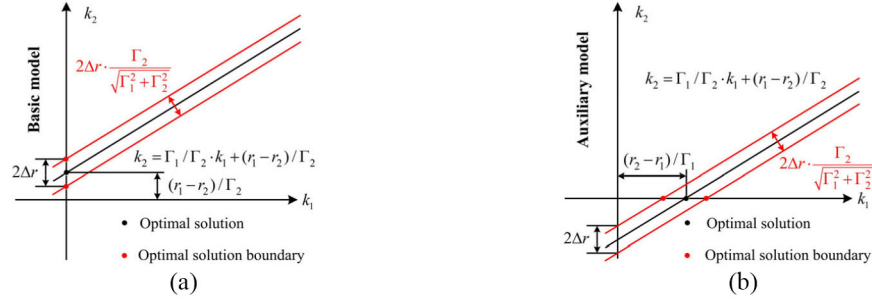
Fig. 3. RPIP model segmentation. (a) Basic model with optimal solution in k_2-axis. (b) Auxiliary model with optimal solution in k_1-axis.

To vividly illustrate this method, Fig. 1 shows the schematic of the RPIP model under the dual baseline, with constraint condition $|\Gamma_1 k_1 - \Gamma_2 k_2 - r_2(s) + r_1(s)| \leq \Delta r$. The black line represents the original linear constraints, and the red line represents the extended boundary constraints introduced by Δr, which makes the feasible domain of ambiguity set slack.

A. Determination and Allocation of Δr

The Δr is related to the tolerance of phase noise in the RPIP model. The smaller the Δr, the poor the anti-noise ability of the RPIP, while too large of Δr may lead to the integer solutions be consistent, hence, a large PU deviation is achieved in the final results. Considering that Δr is associated with intercept, the determination includes two steps. First, the intercept cluster is extracted with refer to the CA-MBPU method. Then, the adjacent intercept clusters are differentiated, and half of the minimum difference is taken as the reference value of Δr, and its calculation formula is as follows:

$$P_i = \text{Peak[Intercept]} \qquad (i = 1, 2, \ldots, t)$$
$$\Delta r_j = \begin{cases} (P_{j+1} - P_j)/2 & (j = 1) \\ (P_{j+1} - P_{j-1})/4 & (j = 2, \ldots, t-1) \\ (P_j - P_{j-1})/2 & (j = t) \end{cases} \qquad (6)$$

where Peak[·] is the expression of extracting intercept cluster, and t is the total number of intercept clusters. Fig. 2 shows the schematic of determining Δr_j.

The allocation of Δr_j can be assigned in the range of the intercept, that is, which interval the intercept value meets is assigned the relative Δr_j

$$\text{Intercept} \in \begin{cases} \left[P_j - \frac{P_{j+1}-P_j}{2}, P_j + \frac{P_{j+1}-P_j}{2} \right] & (j = 1) \\ \left[P_j - \frac{P_j-P_{j-1}}{2}, P_j + \frac{P_{j+1}-P_j}{2} \right] & (j = 2, \ldots, t-1) \\ \left[P_j - \frac{P_j-P_{j-1}}{2}, P_j + \frac{P_j-P_{j-1}}{2} \right] & (j = t). \end{cases}$$
$$(7)$$

B. Searching of the Ambiguity Set

After determining Δr, searching of the ambiguity set is divided into two steps. First, separating the RPIP model into the basic model and the auxiliary model according to the location of the optimal solution [22]. The optimal solutions in the different models are $[0, (r_1 - r_2)/\Gamma_2]$ and $[(r_2 - r_1)/\Gamma_1, 0]$, respectively, as shown in Fig. 3.

Second, considering whether there are integer values in the feasible region interval on the k_i-axis (as shown in the range of red points in Fig. 3), the extraction of integer value for the above two models is as follows:

$$\text{Basic} : \text{INT}\left[\frac{r_2 - r_1}{\Gamma_1} - \Delta r, \frac{r_2 - r_1}{\Gamma_1} + \Delta r \right]$$
$$\text{Auxiliary} : \text{INT}\left[\frac{r_1 - r_2}{\Gamma_2} - \Delta r \cdot \frac{\Gamma_2}{\Gamma_1}, \frac{r_1 - r_2}{\Gamma_2} + \Delta r \cdot \frac{\Gamma_2}{\Gamma_1} \right]$$
$$(8)$$

where $\text{INT}[a, b]$ is the expression of extracting integer in the interval $[a, b]$. The extracted integer combined with 0 is directly the ambiguity set. If this interval has no integer value, the optimal solution is rounded as the starting integer value, and then the ambiguity set is obtained by traversing.

In fact, the traversal starting points in the positive and negative intervals in the RPIP model are consistent, and only the traversal direction is opposite. For simplicity, the search of the ambiguity set is only explained in the positive interval.

Notably, the RPIP method is a pixel-by-pixel PU method. For the pixel-by-pixel PU of the entire interferogram, the time cost of searching the ambiguity set needs to be considered. Therefore, the slope Γ_1/Γ_2 is used to determine the traversal search direction to reduce the time cost, as shown in Fig. 4. For vertical traversal, k_2 is taken as the independent variable, unit length is increased successively from the starting integer value, and k_1 is solved by substituting k_2 into the central constraint condition to be rounded. Then, the ambiguity set candidate $[k_1, k_2]$ is substituted into the threshold distance criterion of (5) to determine the ambiguity set. Similarly, for horizontal traversal, k_1 is taken as the independent variable to traverse and search the ambiguity set. The ambiguity integer values of different traversal directions in the basic model and the auxiliary model are listed in Table I. ($\lfloor \cdot \rfloor$ is the integer operation.)

IV. Performance Analysis

In this section, the performance of the RPIP method is tested by using the simulated and real InSAR data. The first experiment tests the PU feasibility of the RPIP method. The second experiment tests the PU accuracy of the RPIP method, especially the accuracy of the searching ambiguity set. The third experiment tests the DEM reconstruction performance of the RPIP method on a real MB-InSAR dataset.
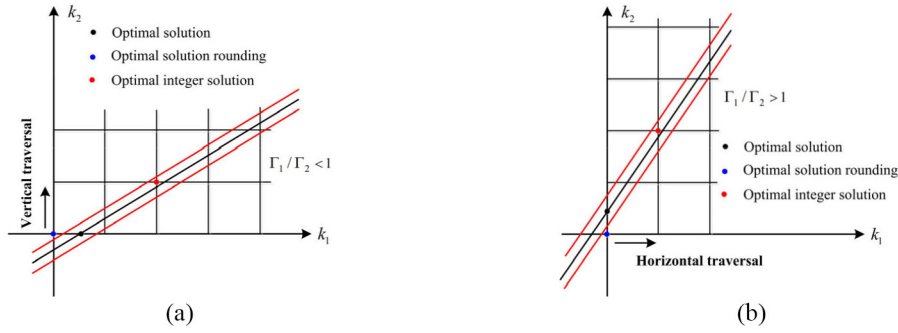
Fig. 4. Traversal determination. (a) Vertical traversal when $\Gamma_1/\Gamma_2 < 1$. (b) Horizontal traversal when $\Gamma_1/\Gamma_2 > 1$.

TABLE I
AMBIGUITY INTEGER VALUES OF DIFFERENT TRAVERSAL DIRECTIONS IN THE BASIC MODEL AND THE AUXILIARY MODEL

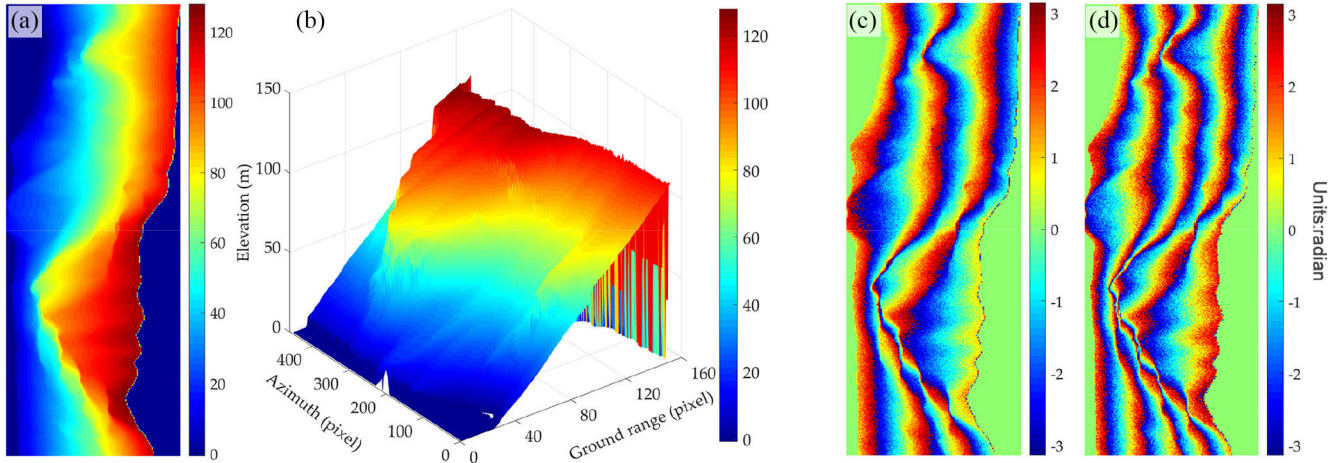| Model	Optimal solution	Slope	Traverse	Direction	Initial ambiguity integer value	Another ambiguity integer value
Basic model	$[0,(r_1-r_2)/\Gamma_2]$	<1	k_2	Vertical	$\lfloor (r_1-r_2)/\Gamma_2 \rfloor$	$\lfloor \Gamma_2/\Gamma_1 \cdot k_2 + (r_1-r_2)/\Gamma_1 \rfloor$
		>1	k_1	Horizontal	0	$\lfloor \Gamma_1/\Gamma_2 \cdot k_1 + (r_2-r_1)/\Gamma_2 \rfloor$
Auxiliary model	$[(r_2-r_1)/\Gamma_1,0]$	<1	k_2	Vertical	0	$\lfloor \Gamma_2/\Gamma_1 \cdot k_2 + (r_1-r_2)/\Gamma_1 \rfloor$
		>1	k_1	Horizontal	$\lfloor (r_2-r_1)/\Gamma_1 \rfloor$	$\lfloor \Gamma_1/\Gamma_2 \cdot k_1 + (r_2-r_1)/\Gamma_2 \rfloor$

Fig. 5. Long's peak DEM and simulated data. (a) 2-D DEM. (b) 3-D DEM. (c) Simulated short baseline interferogram. (d) Simulated long baseline interferogram.

TABLE II
MAJOR PARAMETERS OF THE SIMULATED INTERFEROGRAMS

Orbit Altitude	Incidence Angle	Image Size	Wavelength	Baseline 1	Baseline 2
570km	10.5°	458*152 pixels	0.057m	30m	42m

A. Simulated Data

The first experiments were simulated using DEM data of Long's Peak National Park in the United States, and the corresponding 3-D images are shown in Fig. 5(a) and (b). Based on this DEM, multibaseline interferograms were simulated, with the main parameters listed in Table II. Fig. 5(c) and (d) shows the noise interferograms of different baseline lengths. Analyzing the terrain, there is an obvious terrain mutation area on the right, which provides conditions for testing the unwrapping performance of different algorithms in this area.

Fig. 6(a)–(f) shows PU results of Branch cut, Quality guided, LS, MCF, CA, and RPIP algorithms. The corresponding PU results and the deviation from the reference phase are shown in Fig. 6(g)–(l). It can be seen that the Branch cut, Quality guided, and MCF methods have a clear error band in the large gradient changing terrain, which is due to the fact that the large gradient changing region does not meet the phase continuity condition, leading to PU errors in this area. From Fig. 6(c) and (i), it can be seen that the LS method ensures the continuity of global PU to a certain extent, but this leads to an overall unwrapping error in areas with discontinuous
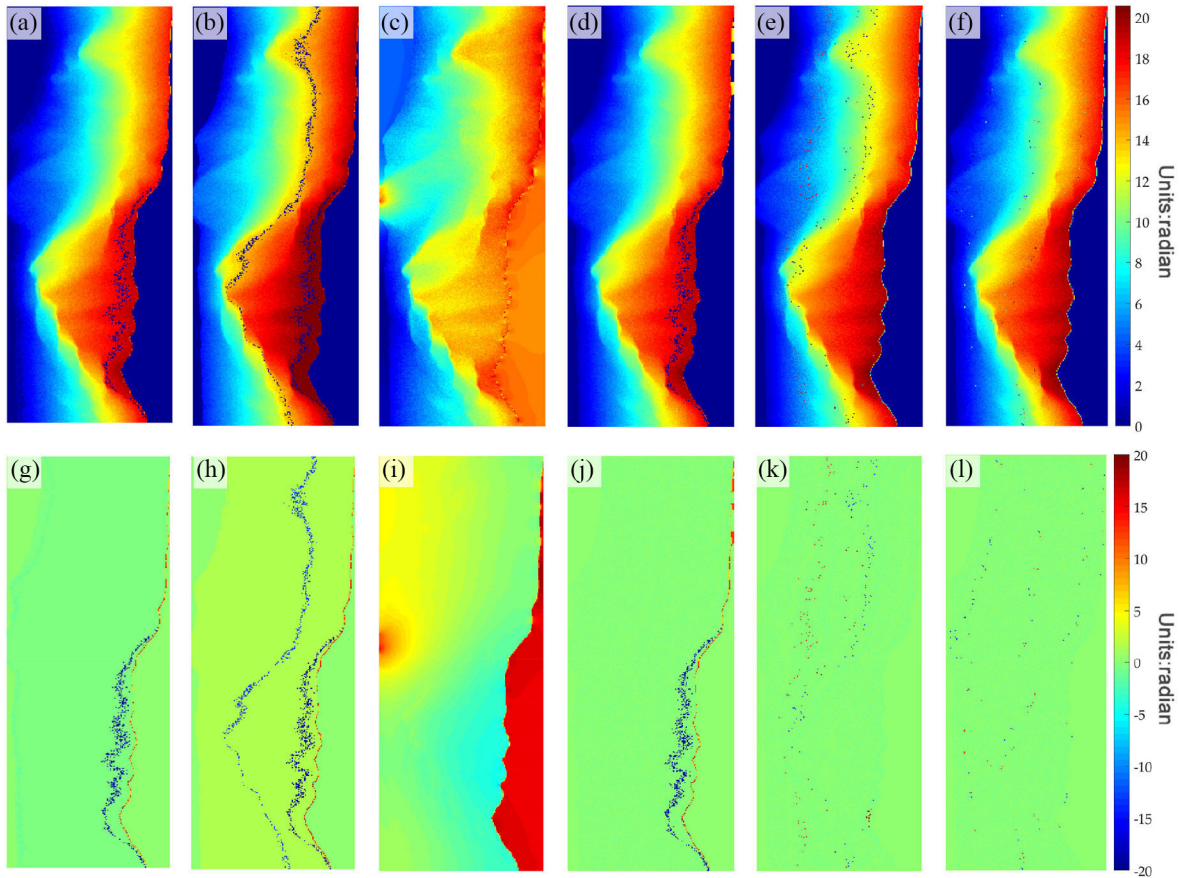
Fig. 6. PU results of different algorithm. (a)–(f) Branch cut, Quality guided, LS, MCF, CA, and RPIP algorithm PU results. (g)–(l) Branch cut, Quality guided, LS, MCF, CA, and RPIP algorithm PU errors.

original terrain, which is not consistent with the original terrain. Due to the influence of noise, the CA algorithm may experience uneven allocation of ambiguity sets at the phase mutation boundary, resulting in some misunderstandings and entanglements in this area. The RPIP algorithm expands the range of clusters and reduces the possibility of noise leading to misinterpretation. Overall, the PPIP algorithm performs the best in unwrapping.

In order to quantitatively verify the PU performance of different algorithms, Table III shows the mean and root-mean-square error (RMSE) of PU error. Overall, the mean phase error and RMSE of the RPIP algorithm are both the lowest, and its unwrapping performance is the best. This is consistent with the unwrapping results, which also proves the feasibility and effectiveness of the RPIP MBPU algorithm.

The second experiment is performed on complex terrain through simulation data in Guatemala. Fig. 7(a) shows the Google Earth image of the study area. Fig. 7(b) shows the DEM of the study area. The simulated noisy interferograms of different baselines (short baseline: 24 m, long baseline: 47 m) by using this DEM are shown in Fig. 8(a) and (b). Fig. 8(c) is the reference phase of Fig. 8(b). Fig. 8(d)–(h) presents the PU results of the branch-cut, MCF, CA, PIP, and RPIP methods for Fig. 8(b). Fig. 8(i)–(m) shows the PU errors between Fig. 8(c) and (d)–(h). It can be seen that the PU results of branch-cut and MCF have significant phase

TABLE III
EVALUATION OF DIFFERENT PU ALGORITHMS FOR 30-m
BASELINE INTERFEROGRAM

Method	Mean/rad	RMSE/rad
Branch-cut	-1.2245	2.2319
Quality-guided	1.4853	2.6496
LS	3.8515	4.7772
MCF	0.8604	1.9571
CA	0.4869	1.7456
RPIP	0.2142	1.0893

errors in the fringe destruction region, which is caused by the difficulty in satisfying the phase continuity assumption in this region. The CA method has patchy phase errors, which may be caused by the same ambiguity set assigned to adjacent cluster intercepts. The PIP method uses the single linear constraint to search the ambiguity set, which may deviate from the reality and lead to the failure of unwrapping, while the RPIP method improves the PU accuracy by extending the feasible region, whose RMSE is the smallest compared with other methods, which proves that the RPIP method can be applied to PU of complex terrain.

In order to further compare the PU performance of the PIP and the RPIP methods, ambiguity 3-D maps of the two methods are drawn in Fig. 9. Burr phenomena can be obviously seen in the PIP method, while the RPIP method has better continuity, which indicates that the number of
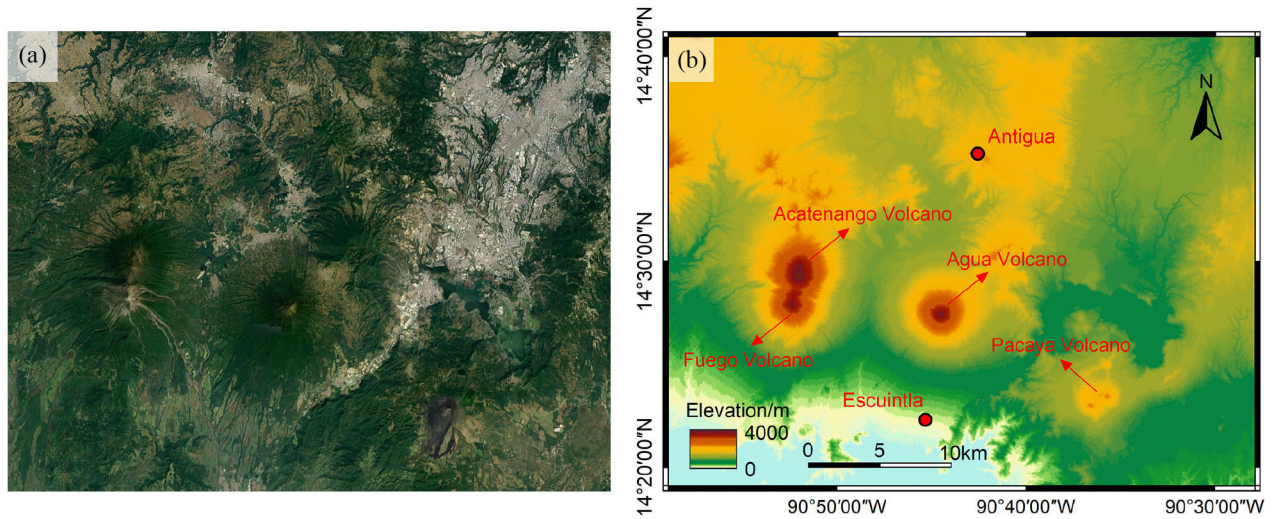
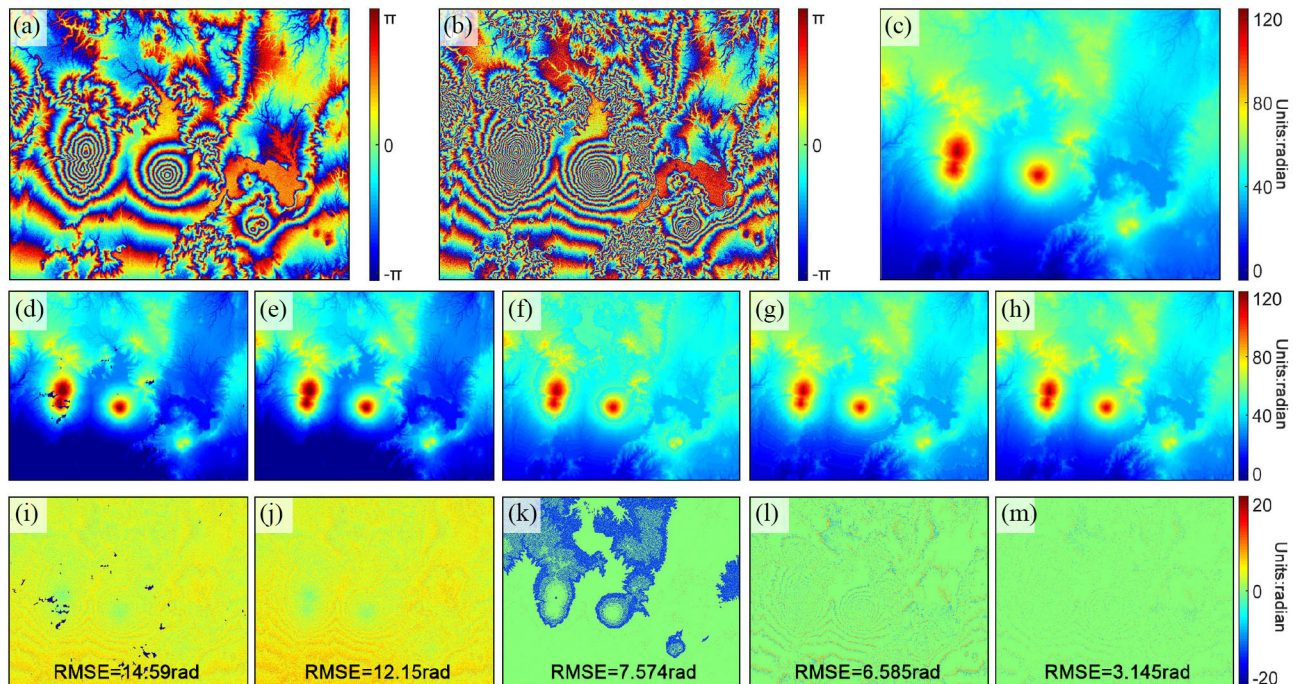Fig. 7. Study area. (a) Google Earth image. (b) PALSAR DEM.

Fig. 8. PU results of simulated data. (a) Simulated short baseline interferogram. (b) Simulated long baseline interferogram. (c) Reference phase of long baseline interferogram. (d)–(h) PU results of branch-cut, MCF, CA, PIP, and RPIP methods. (i)–(m) PU errors of branch-cut, MCF, CA, PIP, and RPIP methods.

phase mutations of the RPIP method is less than that of the PIP method. Table IV lists the residue information of the two methods. The error percentage of the RPIP method is reduced by about 50%. Both quantitative and qualitative analysis results show that the RPIP method has higher PU accuracy.

B. Real Data

The DEM reconstruction of the RPIP method is tested on a TanDEM-X MB data. Fig. 10(a) shows the PALSAR DEM of the study area in Bam, Kerman Province, Iran. Two single-pass InSAR interferograms, with baselines of 496.23

and 586.99 m are shown in Fig. 10(b) and (c). Fig. 10(d)–(h) shows the unwrapped interferograms using branch-cut, MCF, CA, PIP, and RPIP methods. Fig. 10(i)–(m) shows the difference between the reconstructed DEM and the reference DEM with different methods. It can be seen that the remses of the five algorithms are 5.784, 4.029, 1.157, 1.817, and 1.011 m, respectively. Visually, the RPIP method does not exhibit the error accumulation phenomenon of branch-cut and MCF SBPU methods, and the PU effect has good continuity. Moreover, the PU error of this method mainly comes from the deviation of the misunwrapping point. Compared with CA and PIP MBPU, RPIP MBPU greatly reduces the number of misunwrapping points.
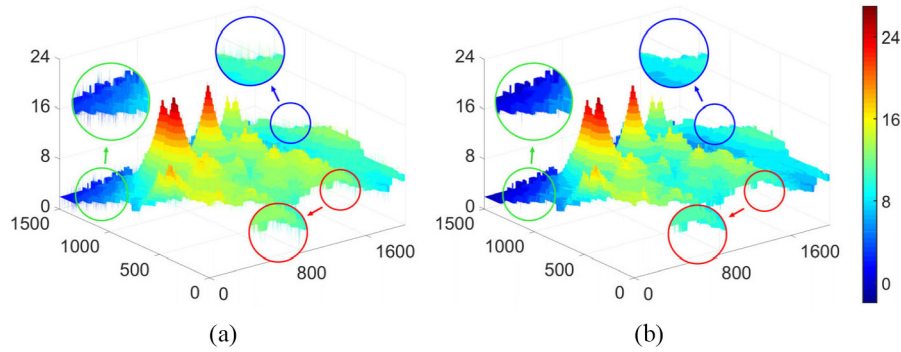
Fig. 9. Ambiguity 3-D map of different methods. (a) Ambiguity 3-D map of the PIP method. (b) Ambiguity 3-D map of the RPIP method.

TABLE IV
NUMBER OF POSITIVE AND NEGATIVE RESIDUES AND ERROR PERCENTAGE OF PIP AND RPIP METHODS

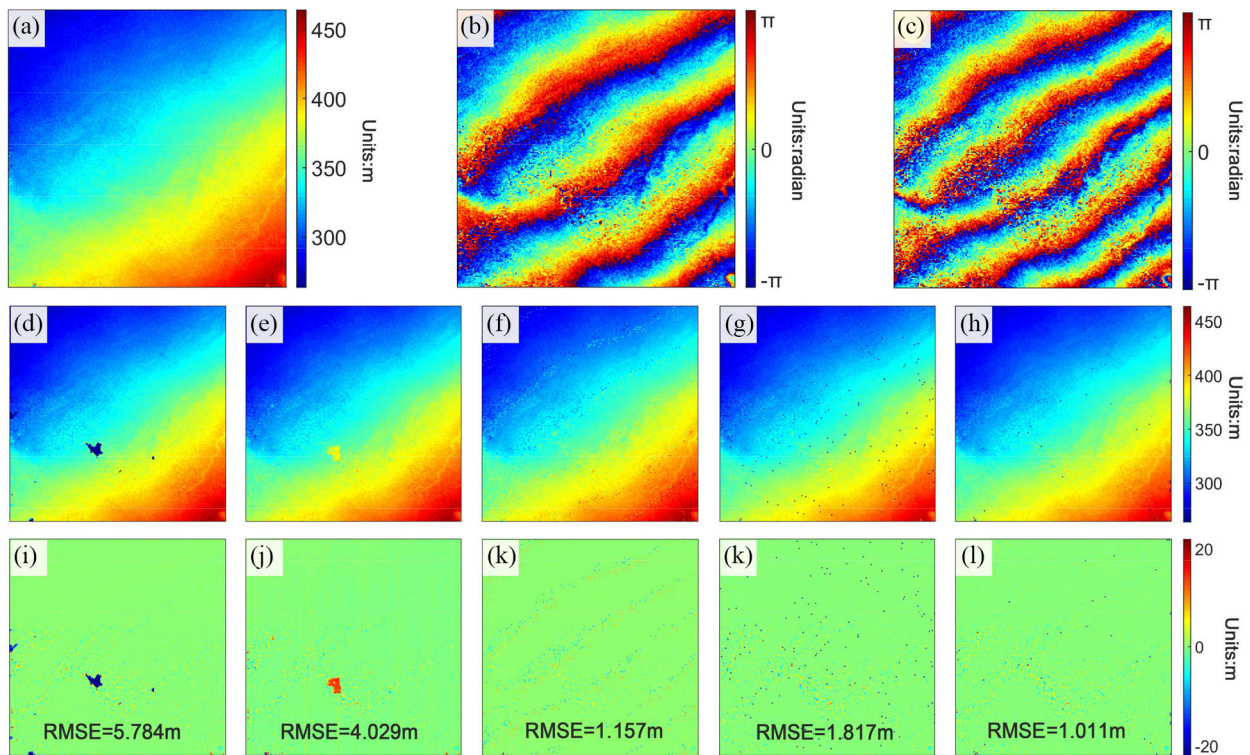| Methods	Positive residues	Negative residues	Error percentage
PIP	60162	57611	3.93%
RPIP	27959	26893	1.83%

Fig. 10. DEM reconstruction results of real data. (a) Reference DEM (m). (b) Short baseline interferogram. (c) Long baseline interferogram. (d)–(h) DEM reconstruction results of branch-cut, MCF, CA, PIP, and RPIP methods. (i)–(m) DEM reconstruction errors of branch-cut, MCF, CA, PIP, and RPIP methods.

In order to further analyze the DEM reconstruction performances, Fig. 11 shows the frequency histogram of DEM reconstruction errors. It can be seen that the frequency that the DEM reconstruction error of the RPIP method falls into the interval $(-1, 1]$ is 86.15%, which is higher than other methods, indicating that the PU results have less deviation. The mathematical expectation μ of Gaussian fitting in the RPIP method is the smallest, which also verifies the RPIP method can obtain better results. Comparing the error distribution between Fig. 10(l) and (m), it can be found that the DEM error caused by the deviation from the true ambiguity set is close to -20 m (represented by the frequency with the error center of -18 m in Fig. 11). Compared with the PIP method, the RPIP method reduces the frequency of misunwrapping by about 60%, which shows that the RPIP method can effectively reduce the probability of misunwrapping, and obtain higher precision DEM.
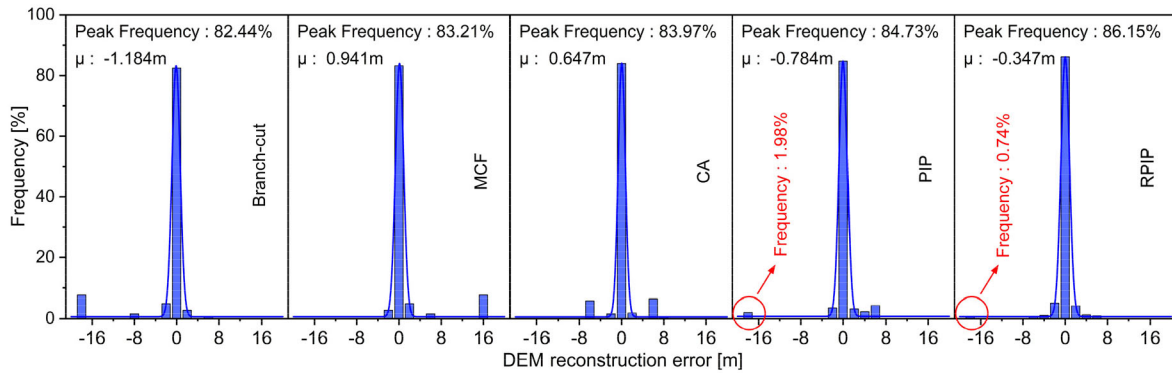
Fig. 11. Frequency histograms of DEM reconstruction error with different methods.

V. CONCLUSION

In this article, an RPIP MBPU method is proposed. The proposed method, which exploits the intercept information of the interferometric phase, introduced a new parameter to extend the feasible domain, and reduce the influence of phase noise. Moreover, the proposed method can obtain more accurate ambiguity set by combining threshold criterion. The experimental results of simulated and real data show that the RPIP method has better PU accuracy. Compared with the PIP method, the number of misunwrapping points in the RPIP method is reduced by about 60%, which indicates that the proposed method can reduce search deviation of the ambiguity set caused by phase noise. In future work, we will pay more attention to the PU efficiency and use the downsampling or fusion cluster-wise unwrapping method of the CA algorithm to improve the PU efficiency.

REFERENCES

[1] M. Xing, V. Pascazio, and H. Yu, "A special issue on synthetic aperture radar interferometry," *IEEE Geosci. Remote Sens. Mag.*, vol. 8, no. 1, pp. 6–7, Mar. 2020.

[2] D. C. Ghiglia, *Two-Dimensional Phase Unwrapping: Theory, Algorithms, and Software*. New York, NY, USA: Wiley, 1998.

[3] Y. Lan, H. W. Yu, Z. H. Yuan, and M. D. Xing, "Comparative study of DEM reconstruction accuracy between single- and multibaseline InSAR phase unwrapping," *IEEE Trans. Geosci. Remote Sens.*, vol. 60. pp. 1–11, Jan. 2022.

[4] H. Yu and X. Hu, "Knowledge-aided InSAR phase unwrapping approach," *IEEE Trans. Geosci. Remote Sens.*, vol. 60. pp. 1–8, 2022.

[5] K. Itoh, "Analysis of the phase unwrapping algorithm," *Appl. Opt.*, vol. 21, nos. 1–4, pp. 2470, Jul. 1982.

[6] Y. Gao et al., "A phase slicing 2-D phase unwrapping method using the L1-norm," *IEEE Geosci. Remote Sens. Lett.*, vol. 19, pp. 1–5, 2022.

[7] Z. Ma, S. Wei, Y. Aoki, J. Liu, and T. Huang, "A new spatiotemporal InSAR tropospheric noise filtering: An interseismic case study over central san Andreas fault," *IEEE Trans. Geosci. Remote Sens.*, vol. 60, pp. 1–16, Sep. 2022.

[8] X. Xie, "Iterated unscented Kalman filter for phase unwrapping of interferometric fringes," *Opt. Exp.*, vol. 24, no. 17, pp. 18872–18897, Aug. 2016.

[9] Y. Gao, S. Zhang, T. Li, Q. Chen, X. Zhang, and S. Li, "Refined two-stage programming approach of phase unwrapping for multi-baseline SAR interferograms using the unscented kalman filter," *Remote Sens.*, vol. 11, no. 2, p. 199, Jan. 2019.

[10] H. Yu, Y. Lan, Z. Yuan, J. Xu, and H. Lee, "Phase unwrapping in InSAR A review," *IEEE Geosci. Remote Sens. Mag.*, vol. 7, no. 1, pp. 40–58, Mar. 2019.

[11] V. Pascazio and G. Schirinzi, "Multifrequency InSAR height reconstruction through maximum likelihood estimation of local planes parameters," *IEEE Trans. Image Process.*, vol. 11, no. 12, pp. 1478–1489, Dec. 2002.

[12] G. Poggi, A. R. P. Ragozini, and D. Servadei, "A Bayesian approach for SAR interferometric phase restoration," in *Proc. IEEE Int. Geosci. Remote Sens. Symp. (IGARSS)*, 2000, pp. 3202–3205.

[13] G. Ferraiuolo, F. Meglio, V. Pascazio, and G. Schirinzi, "DEM reconstruction accuracy in multichannel SAR interferometry," *IEEE Trans. Geosci. Remote Sens.*, vol. 47, no. 1, pp. 191–201, Jan. 2009.

[14] W. Xu, E. C. Chang, L. K. Kwoh, H. Lim, and W. C. A. Heng, "Phase-unwrapping of SAR interferogram with multi-frequency or multi-baseline," in *Proc. IEEE Int. Geosci. Remote Sens. Symp. (IGARSS)*, 1992, pp. 730–732.

[15] H. Zhang, G. Jin, Q. Xu, Z. Qin, and W. Sun, "Application of Chinese remainder theorem in phase unwrapping for dual-baseline InSAR," *Acta Geodaeticaet Cartogr. Sinica*, vol. 40, no. 6, pp. 770–777, 2011.

[16] W. J. Wang and X. G. Xia, "A closed-form robust Chinese remainder theorem and its performance analysis," *IEEE Trans. Signal Process.*, vol. 58, no. 11, pp. 5655–5666, Nov. 2010.

[17] Z. Yuan, Y. Deng, F. Li, R. Wang, G. Liu, and X. Han, "Multichannel InSAR DEM reconstruction through improved closed-form robust Chinese remainder theorem," *IEEE Geosci. Remote Sens. Lett.*, vol. 10, no. 6, pp. 1314–1318, Nov. 2013.

[18] Z. Jiang, J. Wang, Q. Song, and Z. Zhou, "Multibaseline phase unwrapping through Robust Chinese remainder theorem," in *Proc. 7th IEEE Int. Symp. Microw., Antenna, Propag., EMC Technol. (MAPE)*, 2017, pp. 462–466.

[19] H. Yu, Z. Li, and Z. Bao, "A cluster-analysis-based efficient multibaseline phase-unwrapping algorithm," *IEEE Trans. Geosci. Remote Sens.*, vol. 49, no. 1, pp. 478–487, Jan. 2011.

[20] H. Liu, M. Xing, and Z. Bao, "A cluster-analysis-based noise-robust phase-unwrapping algorithm for multibaseline interferograms," *IEEE Trans. Geosci. Remote Sens.*, vol. 53, no. 1, pp. 494–504, Jan. 2015.

[21] Z. Jiang, J. Wang, Q. Song, and Z. Zhou, "A refined cluster-analysis-based multibaseline phase-unwrapping algorithm," *IEEE Geosci. Remote Sens. Lett.*, vol. 14, no. 9, pp. 1565–1569, Sep. 2017.

[22] Z. Yuan, Z. Lu, L. Chen, and X. Xing, "A closed-form robust cluster-analysis-based multibaseline InSAR phase unwrapping and filtering algorithm with optimal baseline combination analysis," *IEEE Trans. Geosci. Remote Sens.*, vol. 58, no. 6, pp. 4251–4262, Jun. 2020.

[23] L. Zhou, H. Yu, Y. Lan, S. Gong, and M. Xing, "CANet: An unsupervised deep convolutional neural network for efficient cluster-analysis-based multibaseline insar phase unwrapping," *IEEE Trans. Geosci. Remote Sens.*, vol. 60, pp. 1–15, 2022.

[24] H. Liu, M. Xing, and Z. Bao, "A novel mixed-norm multibaseline phase-unwrapping algorithm based on linear programming," *IEEE Geosci. Remote Sens. Lett.*, vol. 12, no. 5, pp. 1086–1090, May 2015.

[25] H. Yu and Y. Lan, "Robust two-dimensional phase unwrapping for multibaseline SAR interferograms: A two-stage programming approach," *IEEE Trans. Geosci. Remote Sens.*, vol. 54, no. 9, pp. 5217–5225, Sep. 2016.

[26] Y. Lan, H. Yu, and M. Xing, "Refined two-stage programming-based multi-baseline phase unwrapping approach using local plane model," *Remote Sens.*, vol. 11, no. 5, p. 491,Mar. 2019.

[27] H. Yu, T. Yang, L. Zhou, and Y. Wang, "PDNet: A lightweight deep convolutional neural network for InSAR phase denoising," *IEEE Trans. Geosci. Remote Sens.*, vol. 60, pp. 1–9, Nov. 2022.

[28] B. Jin, J. Guo, P. L. Wei, B. F. Su, and D. J. He, "Multi-baseline insar phase unwrapping method based on mixed-integer optimisation model," *Inst. Eng. Technol. Radar Sonar Navig.*, vol. 12, no. 7, pp. 694–701, Jul. 2018.

[29] H. Liu, J. Yue, W. Liu, Q. Huang, G. Li, and M. Liu, "Multi-baseline phase unwrapping with robust branch and bound pure integer programming algorithm," *Opt. Lasers Eng.*, vol. 161, Feb. 2023, Art. no. 107352.

[30] H. Yu and X. Hu, "Knowledge-aided InSAR phase unwrapping approach," *IEEE Trans. Geosci. Remote Sens.*, vol. 60, pp. 1–8, Jan. 2022.

[31] X. M. Xie, Q. N. Zeng, K. F. Liao, and Q. H. Liu, "Efficient phase unwrapping algorithm based on cubature information particle filter applied t o unwrap noisy continuous phase maps," *Opt. Exp.*, vol. 27, no. 7, pp. 9906–9924, Apr. 2019.

[32] H. Liu, J. Yue, Q. Huang, G. Li, and M. Liu, "A novel branch and bound pure integer programming phase unwrapping algorithm for dual-baseline InSAR," *Front. Environ.*, vol. 10, Jun. 2022, Art. no. 890343.

[33] H. Yu, M. Xing, and Z. Yuan, "Baseline design for multibaseline InSAR system: A review," *IEEE J. Miniat. Air Space Syst.*, vol. 2, no. 1, pp. 17–24, Mar. 2021.